Astron. Astrophys. 309, 733–742 (1996)

ASTRONOMY
AND
ASTROPHYSICS

A giant low-ionization nebula associated with a radio galaxy in a forming cluster at z = 0.79*

E. Giraud [1,2], J. Melnick [1], Gopal Krishna [1,3,4], C. Mendes de Oliveira[1], and V.K. Kulkarni [4]

[1] European Southern Observatory, La Silla, Casilla 19001, Santiago, Chile
[2] Observatoire de Marseille, Place Le Verrier, F-13248 Marseille Cedex 4, France
[3] Max-Planck-Institut für Radioastronomie, Auf dem Hügel 69, D-53121, Bonn, Germany
[4] NCRA-TIFR, Poona University Campus, Pune-411007, India

Received 12 April 1995 / Accepted 12 October 1995

Abstract. We report an exceptionally interesting case of a powerful ultra-steep spectrum radio galaxy at z = 0.794 which exhibits an extended emission line region (EELR) of size about 100 kpc. The galaxy, with an I-band magnitude of 20.1, is apparently located in a forming cluster of galaxies, which may itself be part of a larger structure. The cluster identification is supported by the spectroscopic redshifts measured for another two galaxies which are located in the vicinity of the radio galaxy.

The outer radio contours of the S-shaped double radio source show a striking spatial coincidence with the edges of the EELR, suggesting that the latter has formed from cooling of the intracluster medium (ICM) compressed by the radio lobes. We also consider the possibility that the EELR has originated in tidal interactions/mergers among gas-rich galaxies near the cluster core, as hinted by a long filament of stellar material seen to link the radio-loud galaxy with a neighbour object. The EELR is marked by spectacular sharp-edged structures resembling cones of ionizing radiation emanating from the nucleus of the radio galaxy. From the observed large ratio of $[OII]/[OIII] \sim 3$, the excitation level of the EELR is inferred to be very low, consistent with other cluster cooling flow nebula.

The host of the radio source will possibly, once the merging process and the radio activity are over, become the central cD galaxy of the cluster.

Key words: galaxies: active – galaxies: intergalactic medium – radio continuum: galaxies – galaxies: clusters – galaxies: evolution galaxies: 0410-19

1. Introduction

Powerful radio emissions represent short episodes in the lives of some galaxies, including giant galaxies located in rich clusters like 3C 295 (e.g. Dressler & Gunn 1983). Although powerful radio sources are not found exclusively in dense environments, rich clusters at large distances have indeed been discovered from optical follow-up of ultra-steep spectrum radio sources (e.g., 3C 34 at z = 0.69; Mc Carthy 1988) . In fact cooling gas in clusters can provide ideal working surfaces for relativistic outflows from active galaxies (Fabian 1994). This approach can be fruitful at high z since the richness of clusters associated with radio galaxies is found to increase significantly beyond $z \sim 0.4$ (Yates et al. 1989; Hill & Lilly 1991). In the course of our optical study of ultra-steep spectrum radio sources (Gopal Krishna et al. 1992; Melnick et al. 1993), we have so far discovered three spectroscopically confirmed fairly rich clusters at $z > 0.55$. The Molonglo radio source 0410-19 with a flux density of 2.3 Jy at 408 MHz, a spectral index of -1.2, and a redshift $z = 0.794$, which is the subject of this paper, is one of them.

The main goal of the present study is to investigate the nature of emission-line nebulae occurring in a dense medium which also contains expanding lobes of relativistic plasma. It is primarily based on optical broad and narrow-band imaging of the field, low and medium-resolution spectroscopy as well as radio imaging at 5 GHz. In Sect. 2 - 4 we describe the properties of the source including a detailed comparison of the radio and optical structures. The origin of the EELR is discussed in Sect. 5.

2. Observations and results

2.1. Radio observations

A high-resolution map of 0410-19 made at 5 GHz using the VLA is shown in Fig 1. It is superimposed on a narrow band image centered at $[OII]\lambda3727$ line (see Sect. 2.6). Morphologically, the source is found to be a "fat double" which is atypical for such a luminous radio source $P_{5\ GHz} \sim 2.10^{33}\ erg\ s^{-1}\ Hz^{-1}$ The radio source 3C 28, which is known to lie in a cluster with an X-ray luminous halo, has a similar morphology (Feretti et al. 1984). Particularly relevant to the present work is the rotationally symmetric S-shaped morphology of 0410–19. The position

* Based on recent observations made at ESO and at the VLA. The VLA is operated by Associated Universities Inc., under cooperative agreement with the National Science Foundation

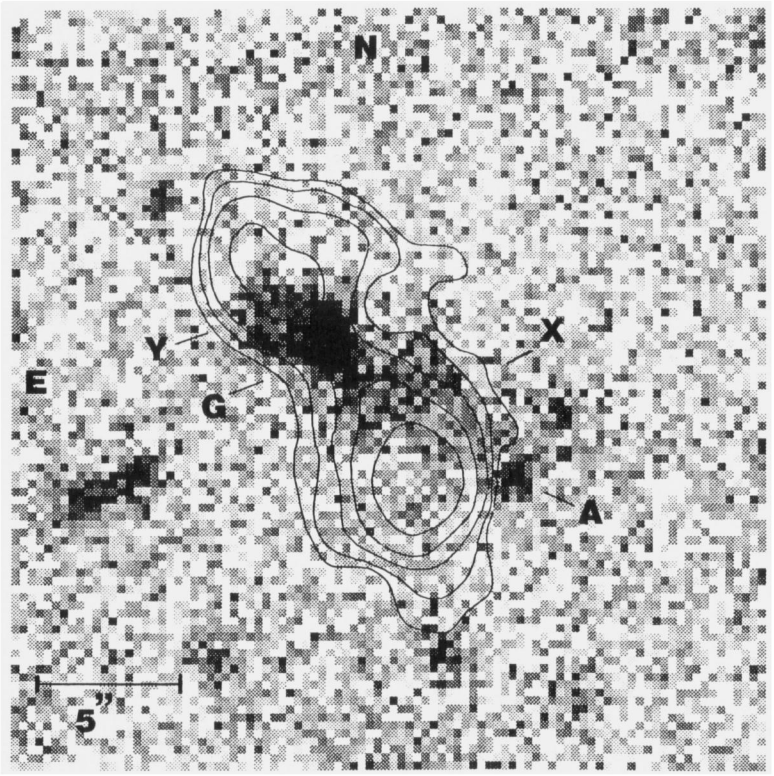

Fig. 1. An $[OII]$ + continuum image taken with a narrow-band filter at 6694 Å (FWHM = 68 Å) of the radio galaxy 0410-19, with 5 GHz radio contours overlaid. North is up, West is to the right. The bar near the lower boundary measures $5''$. The beamwidth of the radio map is $2.3'' \times 1.5''$ north-south, and the contour levels are: 0.5, 1, 2, 4 and 8 mJy per beam. The S-shaped morphology of the "fat-double" radio source is clearly noticeable. The radio isophotes have steeper gradient on the East side of the northern lobe and on the West side of the southern lobe compared to the opposite sides of the respective lobes, suggesting that the radio jets are rotating *anti-clockwise*. The bright regions of nebula are located within the radio lobes, on the sides of steeper gradient in radio intensity. The South-western part of the nebula continues along the radio boundary, all the way to the galaxy A.

angle of the inner radio axis is 35° but, proceeding outward, both lobes show a gradual clockwise bending.

Since radio core remains undetected down to a limit of $\sim 2\ mJy$ at $5\ GHz$ (i.e., $\sim 2\%$ of the integrated flux), we have assumed that the nucleus coincides with the point of rotational symmetry of the inner radio contours. Details of the radio properties will be reported in a separate paper (Kulkarni & Gopal-Krishna, in prep.).

2.2. Broad-band optical imaging

To search for the optical counterpart of the radio source, broad band images in V and R were obtained with EFOSC 1 at the 3.6m telescope with a TeK 512 CCD, giving a scale of $0.61''$ per pixel on the detector. The brightest identified object in the images, hereafter Galaxy G, is found to be extended, with an integrated magnitude of $\sim$ 20.9 in R, and located within an apparent concentration of galaxies.

To detect the stellar population above the 4000 Å break (which occurs at 7175 Å, at the redshift of 0410-19), a 1800 s exposure in the I band was taken with the ESO multimode instrument (EMMI) at the NTT, which is discussed below.

2.3. Continuum morphology and colours

The central part of the $8' \times 8'$ I-band image, obtained with a sampling of $0.27''$ per pixel under $0.8''$ seeing is displayed in Fig. 2b. The central wavelength of this broad band image corresponds to light emitted at 5000 Å in the rest frame of the galaxy, which, because the $[OIII]\lambda5007$ is very weak (Sect. 2.4), is mostly starlight. One clearly notices a chain of faint knots forming a filament linking galaxy G with another galaxy A located $8.5''$ to the southwest. At high contrast the filament is continuous. Its width is $\sim 1.4''$ ($\sim 1.1''$ after a PSF deconvolution). The magnitudes of G and A, are $I = 20.1\pm \sim 0.1$ and $I = 21.3\pm \sim 0.15$ respectively. The corresponding colours are $V - I = 2.1 \pm 0.2$ for galaxy G, which is thus slightly bluer than a passively evolving elliptical at z = 0.8 (models of Guiderdoni & Rocca-Volmerange 1988) and $V - I = 1.7 \pm 0.25$ for A. The filament is bluer by $\triangle(V - I) \approx 0.7 \pm 0.3$ than galaxy G, corresponding to the colour of an Im galaxy at that redshift (same models). Galaxy G is embedded within a large and elongated halo of low surface brightness. This is clearly seen in Fig. 3 which is a contour plot of I band intensity in logarithmic scale. The halo is extended to the northeast and southwest of G and seems to have some sub-structure. G has a faint companion $3.5''$ to the west and Galaxy A has a companion $2.4''$ to the North and another very faint one located $2.5''$ at position angle 300°.

2.4. Low-resolution slit spectroscopy

Three low resolution spectra, 3600 s each, were obtained with EFOSC1 at the 3.6m, using a TeK 512 CCD, in combination with the R300 grism, through a $2''$ slit oriented to cover galaxies G and A. The spectral coverage was from 5940 Å to 9770 Å at a resolution of 24.5 Å. The sky-substracted median of the three exposures shows an emission line at λ = 6685 Å, clearly visible through G to A, and beyond G to the northeast (insert in Fig. 4, and Fig. 6). We identify this line as $[OII]\lambda3727$ at z = 0.794. This is confirmed by the presence of the H and K absorption

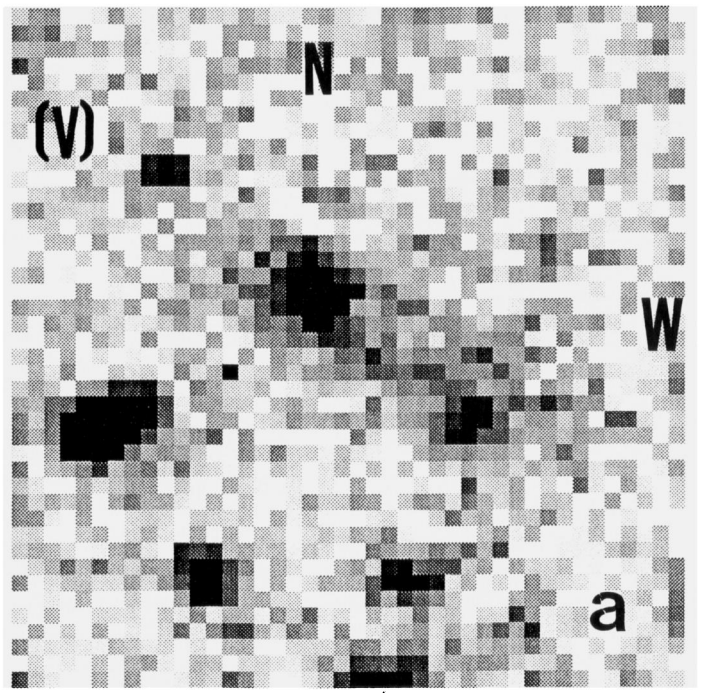

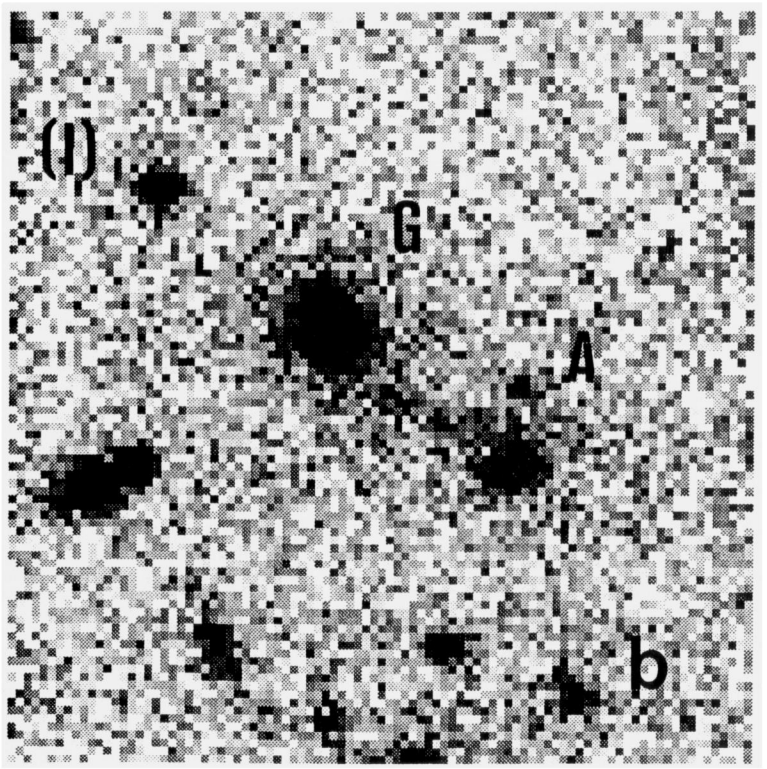

Fig. 2a and b. Broad band images **a** in V and **b** in I of the radio galaxy 0410-19 (G), and another object A, 8.5″ to the southwest. The pixel sizes in V and I are 0.61″ and 0.27″ respectively. The size of the images is 25″ × 25″. North is up, West is to the right. The chain of faint knots between the galaxies G and A appears as a continuous filament at low surface brightness levels. Apparent I-magnitudes of G and A are 20.1 and 21.3 respctively. The filament is significantly bluer than galaxy G (Sect. 2.3).

lines of Ca II and the 4000 Å break (Fig. 4 and Table 1). The overall extent of the $[OII]$ line seen in the spectrum is 13″ which corresponds to 90 h^{-1} kpc, where $H_o = 75$ h km s^{-1} Mpc^{-1}. At the position of galaxy A, the $[OII]$ emission becomes weak, but is clearly visible at the same redshift. A spectrum of a third galaxy falling along the slit, marked B on Fig. 1, gives a redshift of z= 0.79, supporting the cluster interpretation. For yet another galaxy located 20″ southwest of G (1 mag bluer than G), we measure a redshift of 0.601 from $[OII]$ and $[OIII]$ emission lines, placing it clearly in the foreground. The colour difference between galaxy G and the bright knot located between G and A is confirmed by taking the ratios of the continuum levels measured on the low resolution spectra at their locations. A similar analysis confirms the $\sim$ 0.7mag bluer colour for the line-emitting "lobe" immediately northeast of G, relative to the galaxy G.

Table 1. Spectrum of 0410-19 and filament

Region	[OII]	H and K	Hβ_{em}	[OIII]λ4958	[OIII]λ5006	I([OII])/I(Hβ)	I([OIII]/I(Hβ)
"lobe"	0.794	0.793	defect	0.791	—	2 - 3:	1 ?
G core	0.794	0.794	0.792:	0.793	—	> 4	1 ?
"patch"	0.793	0.793	0.792	0.792	0.793	$\approx 3-4$	$\sim 0.5-1$
Gal. A	0.794	0.793	0.793	—	—	—	—

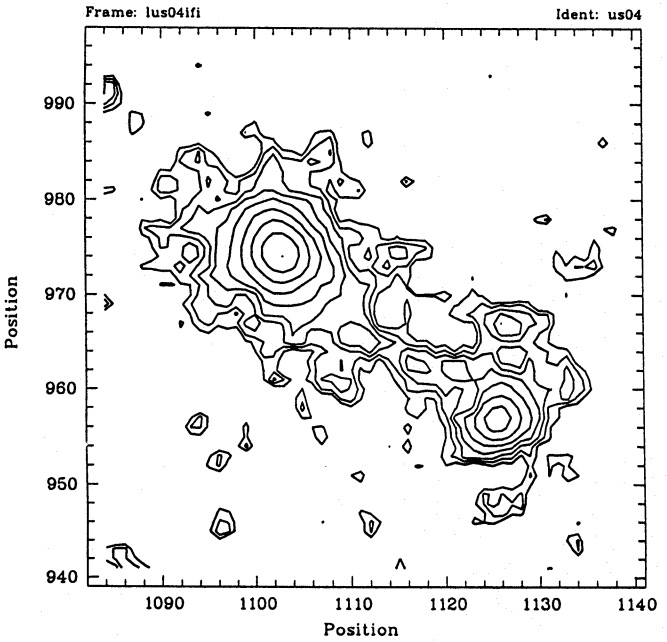

Fig. 3. A contour plot in the I-band of galaxies G (0410-19), A, and the filament, with intensities shown on logarithmic scale. Galaxy G is embedded in a large halo extending to the NE and SW towards the EELR. This contour diagram shows the filament to be continuous with a minimum width of 1.4″ (seeing 0.82″).

2.5. Excitation level of the EELR

In Fig. 4 we display the spectra for three locations along the slit. They coincide with (i) galaxy G, (ii) the bright knot in the filament $\sim$ 3.3″SW of galaxy G, which is within the bright quasi-rectangular "patch" of $[OII]$ emission between G and A (Fig. 5), and (iii) the "lobe" of intense $[OII]$ emission centered $\sim$ 2.7″ northeast of galaxy G. Each of the spectra is an average over 3 consecutive rows along the slit. The large values of the line intensity ratios $[OII]/[OIII]$ and $[OII]/H\beta$ (Table 1) clearly indicate a low state of ionization throughout the nebula. The $H\beta$ emission is more convincingly detected on the two nebular regions ("patch" and "lobe") than on galaxy G (where it is diluted by the absorption of the old stellar population). There is a marginal detection of $H\gamma$ in the NE region ("lobe"), but none from the SW rectangular "patch", suggesting a slightly higher excitation level for the NE nebula. The Ne lines ($[NeIII]$, $[NeV]$) are not detected at any of the locations. While not unusual for off-nuclear spectra (McCarthy 1988), this spectrum is atypical compared to the "average" spectrum of 3C radio galaxies (Spinrad 1986). The low ionization level of the gas is similar to that of some emission-line nebulae associated with central galaxies of cooling flow clusters (e.g., Zwicky 3146, Abell 1835; Allen et al. 1992).

The $[OII]$ flux integrated along the slit is found to be $\sim 1.8.10^{-15}\ erg\ s^{-1}\ cm^{-2}$ with an uncertainty factor of < 2 (the observations were not made in good photometric conditions). From this and the observed extent of the EELR (Fig. 5) we estimate the integrated $[OII]$ luminosity to be $\sim 10^{43}\ h^{-2}\ erg\ s^{-1}$.

The $[OII]$ line is unresolved in velocity and is tilted with a maximum velocity variation of $\approx 700\ km\ s^{-1}$ (Sect. 2.8).

2.6. Narrow-band optical imaging

In order to map the redshifted [OII]λ3727 line-emitting region, a 5400 s narrow-band image through a 68Å wide filter centered at λ = 6694 Å was obtained using EMMI on the NTT. Fig. 1 shows the image together with the radio contours overlaid. From our astrometry, the accuracy of the registration of the radio and optical images is estimated to be 1″. The seeing measured on this image is 0.85″ FWHM which facilitates direct comparison with the I-band image (Fig. 2b). In Fig. 5, the narrow-band image has been smoothed by a boxcar function of 2 × 2 pixels, and displayed with high contrast to reveal the low surface brighness parts of the nebula.

2.7. The extended emission-line region (EELR)

The elongated giant ($\sim$ 13″ $\approx 90\ h^{-1}\ kpc$) EELR has a complex morphology marked by sharp and straight edges. Specifically, there is a triangular-shaped emission-line region extending to the southwest of G, which we will identify below with its radiation cone (Sect. 5.2). The other radiation cone of G is visible to its northeast, referred to above as the "lobe". The emission between G and A consists of two main features: a bright quasi-rectangular patch and a triangular-shaped emission region of lower surface brightness which is seen to extend from the galaxy A to the northeast. The cones must trace the distribution

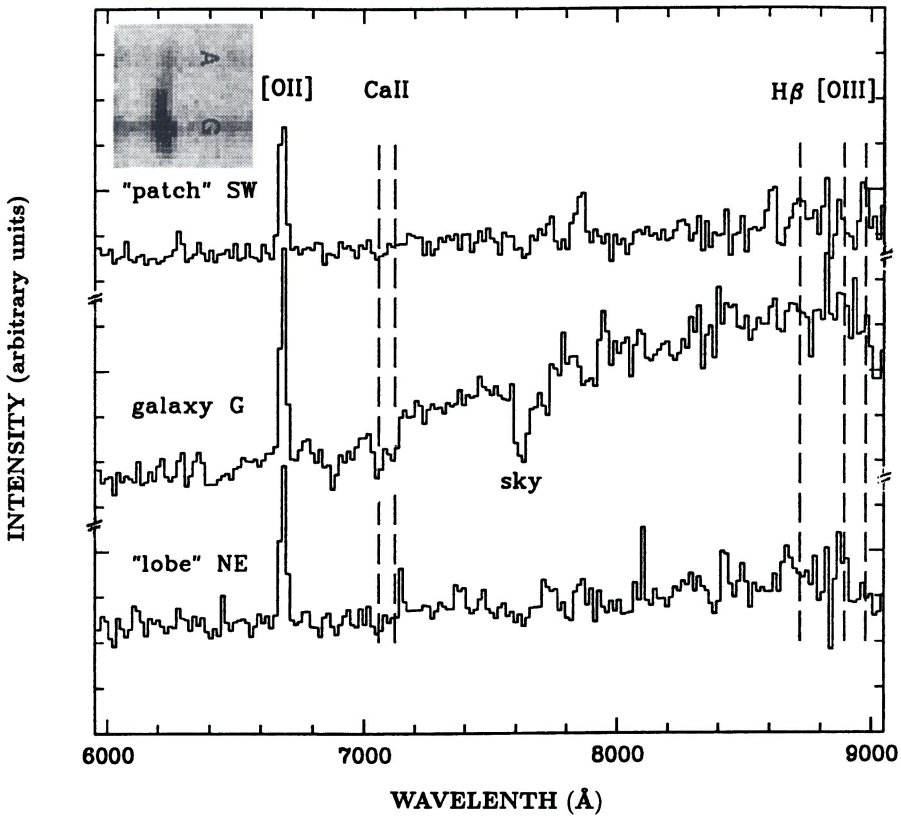

Fig. 4. The low-resolution spectrum along the filament joining galaxies G (0410-19) and A. The inset shows the emission line at $\lambda = 6685$ Å visible all along from A to G, and beyond. The three one-dimensional spectra correspond to the following locations along the slit (see Fig. 5) : (i) the "patch" $\sim 3.3''$ SW of galaxy G, (ii) galaxy G, and (iii) the "lobe" of emission centered $2.7''$ NE of galaxy G. Each of the spectra is an average of three rows along the slit.

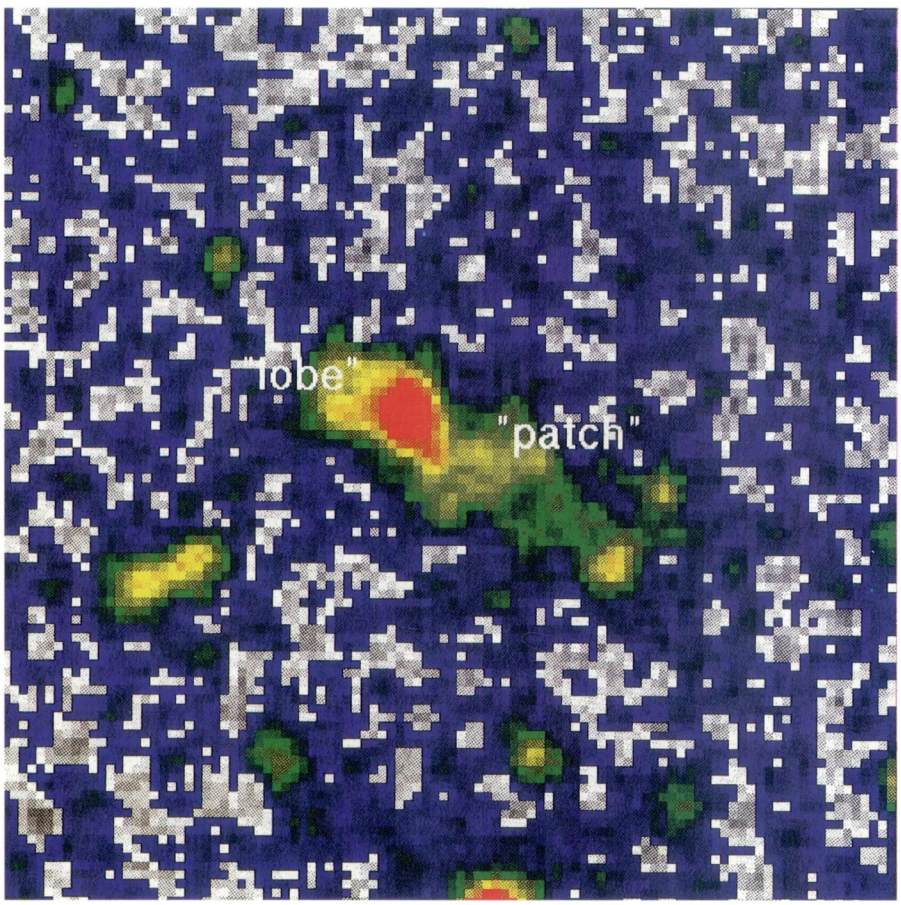

Fig. 5. The same narrow-band image as in Fig. 1 but displayed at high contrast after smoothing. North is up, West is to the right. The regions of the EELR referred to as the "lobe" and the "patch" in the text are identified. In case the EELR is ionized by the radiation cones of the active galaxy G (0410-19), the PA of the axis of the ionizing beams is about 50°.

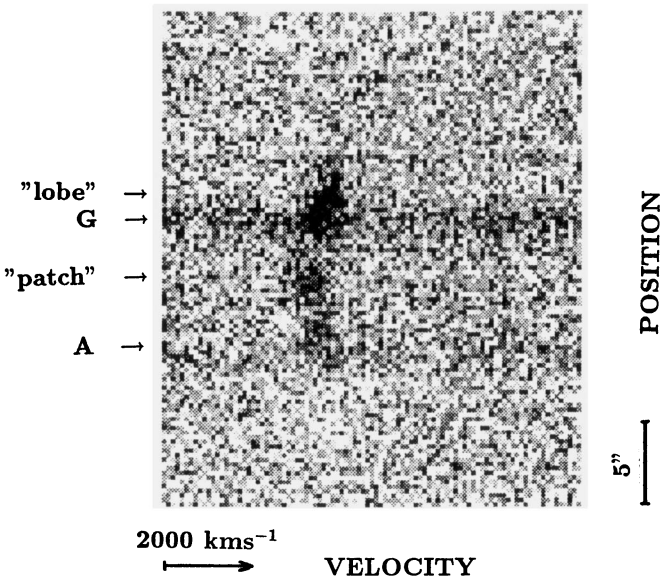

Fig. 6. Velocity-space diagram obtained at an intermediate resolution of 9 Å (FWHM). The 2″ slit was placed along the axis G - A. The continuum of G and A, and the "lobe" and "patch" components of the EELR are indicated. The horizontal arrow corresponds to 2000 km s^{-1}, and the verical bar measures 5″ . The maximum velocity difference across galaxy G is $\sim$ 630 km s^{-1}. The patch is blueshifted by $\sim$ 250 km s^{-1} with respect to G. The emission line is resolved.

of warm gas since in the I-band image only a much narrower filament is seen between galaxies G and A. The colours and spectral properties of the emission-line regions are given in the previous sections.

2.8. The velocity field

In order to obtain kinematical information on the EELR and the galaxies, two 5400 s intermediate-resolution spectra were obtained with the NTT and EMMI at a resolution of 9 Å (FWHM). We used the combination of grism 6 of 1.2 Å/pixel with a two-pixels binning in wavelength and a slit of 2″ aligned along the A - G axis. On the derived two-dimensional spectrum the $[OII]$ line is found to be curved and consisting of three spatial components (Fig. 6). The brightest component extends from the core of the galaxy toward the northeast region ("lobe") and is tilted by 14 Å which corresponds to a total velocity field of $\sim$ 630 $km\ s^{-1}$. The central component corresponds to the rectangular patch, which encompasses the bright knot in the I-band filament (Fig. 2). This component is blueshifted by $\sim$ 250 $km\ s^{-1}$ with respect to the galaxy G. The third component, the faintest one, coincides with the galaxy A.

The velocity-space diagram in Fig. 6 suggests that galaxies G and A have the same velocity and are probably at rest in the potential well of the cluster, while the central part of the EELR seems to be approaching us.

Where it is bright, the $[OII]$ line is found to be resolved, the velocity width corrected for instrumental broadening varying from 400 $km\ s^{-1}$ (FWHM) at the galaxy G to $\sim$ 700 $km\ s^{-1}$ at the rectangular patch beween G and A.

3. Environment of 0410-19

The radio galaxy G (I = 20.1) appears to be located in a rich field of galaxies. However, the field also contains a number of objects with magnitudes similar or brighter than G, which probably belong to the foreground. To quantify the visual impression, we have compared the I-band number counts within a 2′ × 2′ field centered at the radio galaxy (Fig 7a) with those obtained for 3 nearby control fields of the same size, as well as with the counts given by Tyson (1988). The comparison is made for the magnitude interval $20 < I \leq 22$, which also means that we are verifying the hypothesis that the radio galaxy is the first-ranked object in a cluster. We find that the counts in the field of the radio galaxy are nearly twice those in the control fields (51 vs 25, 26 and 23), and also twice the expected Tyson counts. Thus, we infer that the radio galaxy is very likely located in a cluster or a forming cluster. This may provide a clue about the gaseous medium around the radio source.

Another potentially important finding is the existence of two other concentrations of galaxies, also in the magnitude range $20 < I < 22$ seen within the 8′ × 8′ field of the I image. One of them, located 2.1′ North of G, is shown in Fig. 7b. The second lies at 2.4′ from G at $PA \approx 210^o$. In both cases, the cluster-like appearance is more conspicuous (compared with 0410-19) and foreground contamination less marked. In contrast to nearby powerful radio galaxies which tend to avoid regions of higher than average densities (Lilly and Prestage 1987), 0410-19 seems to lie in a very large super-structure. It would be important (also for the understanding of cluster and supercluster formation) to determine if the three apparent clusters belong to a single supercluster at $z \sim 0.8$.

4. Summary of the observed properties of 0410-19

Before proceeding further, we recapitulate the salient properties of this system:

(i) A faint filament with knots, linking two central galaxies of a probable cluster is seen on the I image (G and A; Fig. 2b and Fig. 7a).

(ii) The $[OII]$ emission has sharp edges and extends over nearly 90 $h^{-1}\ kpc$, encompassing the galaxies G and A and extending even beyond G (Fig. 5). This EELR is confined within the radio boundaries and its edges coincide with the outer radio contours of the two lobes (Fig. 1).

(iii) Between galaxies G and A there is a bright quasi-rectangular patch of $[OII]$ emission within which the brightest I-band knot is located (Fig. 5; Fig. 2b).

(iv) The major axis of the galaxy G on the $[OII]$ image has a position angle of $PA \approx 25^o$ (Fig. 5) which is close to that defined by the radio lobes (Fig. 1).

(v) The $[OII]$ line is tilted with a velocity gradient of $\sim$ 630 $km\ s^{-1}$ in the region extending from galaxy G to the northeast "lobe", and at the position of the rectangular patch

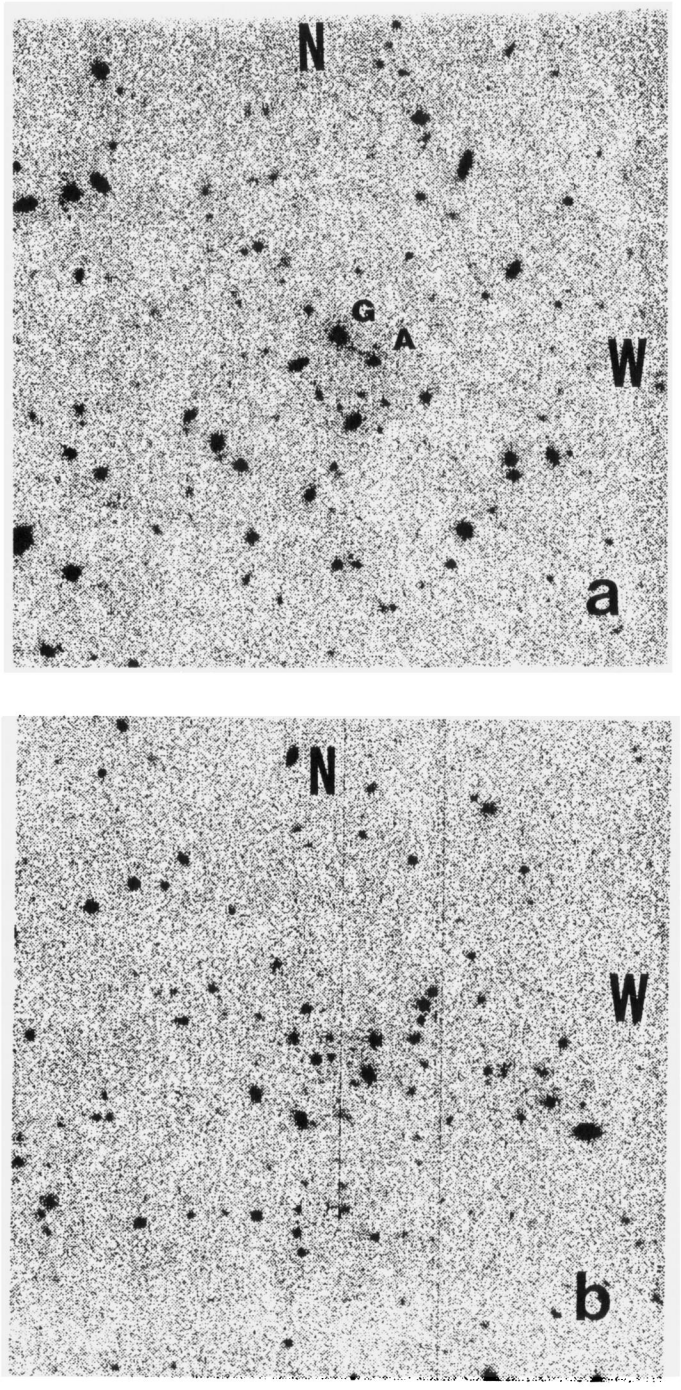

Fig. 7. a A $2' \times 2'$ I-band image centered on 0410-19 (G). The number counts between the magnitude of G (I = 20.1) and I = 22 are nearly double of those in a nearby control field, and also two times those deduced from Tyson (1988) deep survey. This suggests that the radio galaxy lies lies within a cluster or forming cluster at z = 0.8. **b** The $2' \times 2'$ field showing one of the two cluster candidates (located 2.1′ north of G), found within the $8' \times 8'$ I-band image centered on 0410-19.

is blueshifted by $\sim$ 250 $km\ s^1$ with respect to galaxy G. The velocity width varies from 400 $km\ s^{-1}$ at G to 700 $km\ s^{-1}$ at the rectangular patch (Fig. 6).

(vi) The EELR (Fig. 4) has a low level of ionization

(vii) Galaxy G is slightly bluer than a passively evolving elliptical at z = 0.8. The filament is clearly bluer than G and, within the photometric uncertainties, has a $V - I$ colour index similar to that of Im galaxies.

5. The nature of the EELR

Several physical components may contribute to the formation of the observed giant EELR: the radio source with its lobes; the ICM, the gravity between the galaxies G and A; and the progenitors of 0410-19, if it was produced and fuelled through merging. In this section we explore possible scenarios that could account for the observed properties listed above.

Although EELRs (of smaller size) are often detected around central galaxies of (cooling flow) clusters, their origin is currently a much debated issue (Fabian 1994; Baum 1992; Sparks 1992) At low redshifts, the typical sizes of EELR are found to be of the order of the size of the host galaxy (review by McCarthy 1993), so the gas is likely to originate from the interstellar medium of the galaxy (e.g., van Breugel et al. 1985). In contrast, the present EELR extends over almost 100kpc and hence the intra-cluster medium(ICM) is a possible source of the EELR gas. There are a few examples, however, of large EELRs, with size about half 0410-19, which are not located in obvious rich clusters (e.q. 3C 277.3). Since the host galaxy of 0410-19 is located in a rich field, it is also conceivable that interstellar gas has been spread over the large volume due to ongoing gravitational encounters/mergers between gas rich galaxies. One possibility for the formation of the present EELR is that it could be a stream of gas being pulled gravitationaly from its neighbouring galaxy A. The EELR can also be associated with the debris of the encounter, which presumably triggered the radio source. This possibility is discussed in Sect. 5.1.

The merger scenario, however, does not account for the striking spatial coincidence of the EELR with the boundaries of the radio lobes (Fig. 1). This suggests an origin of the EELR from cooling of the intracluster medium compressed by the radio lobes, as discussed in Sect. 5.2.

5.1. Merging

The optical morphological characteristics of 0410-19 are in some ways highly reminiscent of nearby mergers like those clasifed as "Galaxies with tails, loops of material or debris" by Arp and Madore (1987a, AM 0500-590 in 1987b) . Steep surface brightness gradients and sharp edges are witnessed in some of the Arp-Madore objects. Likewise, nearby radio galaxies such as 4C 12.50, 3C 293, PKS 2300-189 (Heckman et al. 1986) exhibit tails and bridges of continuum and emitting material, and very close double nuclei. The merger simulations (Fig. 4a of Hernquist, 1993 in particular) describe well the gross structure of the

EELR in 0410-19 and give us some information about its progenitors, which would be two gas-rich galaxies with prominent bulges (M31-like). The rotations and the approach velocities in the Hernquist model are consistent with the maximum velocity tilt measured across the central body of G (as measured by the $[OII]$ line). The observed velocity width perpendicular to the G - A filament would make this structure vanish over $\sim 10^8\ yr$, if it is not bound, also consistent with Hernquist model. The simulations of Barnes and Hernquist (1991) suggest that in the inner region the gas falls into compact clouds which merge in a rapid inflow to the center, that may be able to fuel an active nucleus (Gunn 1979). As the nuclear activity is ignited it will interact with the embiant medium including any tail drawn out by the strong tidal forces of the merging. Interacting with the expanding radio lobes and irradiated by the nuclear UV photons, such material could then give rise to an EELR (see, e.g., van Breugel et al. 1986; Stockton & MacKenty 1987).

While supported by the arguments above, the merging scenario is unlikely to be the whole story since the geometry of the EELR is found to be cone-like, with edges showing a spatial coincidence with the boundaries of the radio source (Fig. 1). This suggests that the radio source plays a dominant role in the origin of this giant EELR.

5.2. Radio morphology and the EELR

The sharp edges and overall shape of the EELR suggest that we are probably witnessing regions ionized by the radiation cones of the active galaxy G. The position angle of the conical ionization pattern is around 50° which is close to the inner radio axis ($PA \sim 35°$). Since the luminous matter appear to be more concentrated on the side of G facing A, it is conceivable that an asymmetry existed in the distribution of the intra-cluster gas prior to the onset of the radio activity. A bridge of material may have formed due to a gravitational interaction between the two galaxies, or a cooling flow seeded preferrentially on the gravity axis defined by them. The sheaths of gaseous filaments compressed by the radio lobes may reveal this initial asymetry. It is remarkable that the SW component of the EELR follows the side of steeper gradient of the radio isophotes of the southern lobe. This is similar to the case of NGC 1275, where the expanding radio lobes seem to displace the X-ray emitting gas (Bohringer et al. 1993). The straight-edge of the triangular shaped emission line region is most likely due to an obscuring dust-lane around G whose inferred direction would then be almost perpendicular to the inner radio axis.

The low-excitation level of the EELR suggests that the ionized gas is dense, which is consistent with an origin out of the ICM of a still forming cluster, but also the large physical extent of the EELR would cause a dilution of the nuclear photon field. Together, these factors could adequately diminish the ionization parameter to become consistent with the low ionization state of the EELR within models where the AGN radiation is the dominant source of ionization (see, Ferland & Netzer 1983; Halpern & Steiner 1983).

Several possible instances of density enhancement of thermal gas near or around the radio lobes have been reported in the litterature (e.g. van Breugel et al. 1984; Baum & Heckman 1989; Meisenheimer & Hippelein 1992; Gopal-Krishna et al. 1995). Here we consider this possibility for the case of 0410-19, whose radio morphology is marked by an S-symmetry (Fig. 1). Two scenarios are frequently invoked to explain such a morphology. It could either arise due to precession of the nuclear axis (Ekers et al. 1978; Begelman et al. 1984), or due to buoyant advection of the lobe plasma out of a denser embiant ICM (Gull & Northover 1973). In the precession scenario, the jets would be rotating anticlockwise. Hence, the maximum transverse compression of the ICM by the precessing jets would currently be occurring near their leading edges . The same geometry of compression would arise in the buoyancy scenario. The transverse pressure exerted by each radio lobe, as required for its observed clockwise deflection, would be maximum in areas where the lobe's profile shows the largest curvature (marked by X and Y in Fig. 1). In both scenarios a thin sheath of shock-compressed cooling intracluster plasma is expected to form around the radio lobes, particularly near the regions X and Y which mark the maxima in lobe pressure and hence the strongest compression of the ambient ICM.

5.3. Star formation

The compression of the ambient gas by a supersonically expanding radio lobe could also lead to some star formation: depending on the mass and size distribution of the inhomogeneities in the embient gas (e.g. Rees 1989; Begelman & Cioffi 1989). Thus a significant amount of optical continuum can be expected from the region of the nebulosity. It is conceivable that young stars forming in the compressed plasma are an additional source of *in situ* ionization.

Comparing the narrow-band image (Fig. 5) with the I band image (Fig. 2b), we find that the starlight in the filament is displaced with respect to the nebula perpendicular to the G – A axis. In the scenario where the gas is compressed by the precessing radio jets rotating *anticlockwise,* the starlight appears to be back to the nebula as if there is a delay between the gas starting to be ionized and the stars shining. The starlight also seems to avoid the central region of the lobe where, if the case of NGC 1275 applies, there is presumably a cavity in the gas .

5.4. Energetics and dynamics

If we assume 10 % efficiency for the radio emission, the energy injected by the radio source is two orders-of-magnitudes higher than the observed $[OII]$ output of the EELR. Adopting a biconical geometry for this nebula ionized largely by the central AGN, and assuming a filling factor of 10^{-6} to 10^{-7} for the $10^4\ K$ gas, as estimated for cooling flow nebulae (Heckman et al 1989; McCarthy et al., 1990b) we estimate a total mass of $1 - 3.10^8\ M_\odot$ for the gas and a density of $300 - 900\ cm^{-3}$, assuming case B recomination. Although poorly constrained,

such relatively high densities are consistent with the observed low state of excitation.

If the blueshift of the "patch" ($\sim 250\ km\ s^{-1}$) is interpreted as a projected motion of the gas induced by the radio lobes, its kinetic energy would be a very small fraction of the energy content of the radio source. The same would hold for the energy associated with the measured velocity dispersion (700 $km\ s^{-1}$) in the region of the "patch".

5.5. One or two sources of ionization cones?

From the observed geometry of the EELR it seems conceivable that either G alone is responsible for the radiation cones or that both galaxies G and A emit radiation cones. In the latter case the bright rectangular patch of $[OII]$ seen between the two galaxies could be the region where the eastern cone of A overlaps the western cone of G, a possibility consistent with the visual impression of the $[OII]$ image (Fig. 5). Note that since the radio lobe does not extend to the western side of A, the density of thermal plasma to be ionized is not enhanced in that region. The invisibility of the south-western radiation cone of A can thus be simply explained. We notice however that a number of distant radio galaxies have close companion galaxies (Mc Carthy 1988; Miley 1992; Rottgering 1993) which did not lead to this interpretation.

6. Scenario and conclusion

The apparent concentration of faint galaxies in the vicinity of the radio-loud galaxy 0410-19 and the redshift data available on two of its immediate neighbours support the case for the radio galaxy being the dominant member of a very distant cluster or forming cluster.

In the absence of a radio source with large radio lobes, the $\sim 60\ h^{-1}\ kpc$ long filament of stellar material linking this galaxy to its smaller neighbour would have simply suggested that we are witnessing the formation of a first-ranked cluster galaxy through a process of tidal interaction. Due to the rather small separation between galaxies G and A a filament of tidal origin or a gas density enhancement between the two galaxies can be reasonably expected.

The unusually well organized geometry of the EELR and its intimate spatial relationship with the radio source lead us to infer that another process might play an important role in the origin of the EELR. The edges of the EELR and the radio lobes are coincident and, moreover, the most prominent parts of the EELR overlap with the densest regions of the radio isophotes signifying locations of pressure maxima. This suggests that the thermal plasma of the EELR has condensed out of the presumably clumpy embiant medium (ICM) shock-compressed by the expanding radio lobes.

The observed bi-conical geometry of the EELR centered on the radio source indicates that the UV photons from the active nucleus of G are the main source of excitation of the EELR. The low excitation level revealed by the large $[OII]/[OIII]$ ratio could be reproduced by an appropriately small ionization parameter ($U \sim 10^{-4}$) which is not unexpected considering the enormous size of the EELR and its possible location in a dense ICM. Several cooling flow nebulae show similarly low ionization levels (see, Allen et al. 1992),

Since most of our interpration is based on the inferred hypothesis of a dense ICM, it is necessary to prove that 0410-19 is indeed lying in a distant cluster. Photometry of this field should reveal a concentration of very red galaxies (Ellis 1991) and low resolution spectra would be necessary to prove membership. Spectra will also tell us what was the galaxy population in a cluster at this distant redshift. An X-ray detection would reveal the presence of a hot intra-cluster gas. Observing the two neighbouring cluster candidates which may together turn out to be an example of an early formed supercluster, is another exciting possibility presented by this field. Equally crucial would be the morphological study of these distant galaxies using the HST, which forms a currently very active field initiated a few years ago from ground-based imaging observations (Giraud 1992).

Acknowledgements. We thank M. Azzopardi and S. Benetti for the broad band images which they have taken for us.

References

Allen S.W. et al., 1992, MNRAS 259, 67
Arp H., Madore B.F., 1987a, A Catalogue of Southern Peculiar Galaxies and Associations, Cambridge University Press, Vol. 1
Arp H., Madore B.F., 1987b, ——, Vol. 2, Plate 9.4
Barnes J.E., Hernquist L., 1991, ApJ 370, L65
Baum S.A., 1992, in: Fabian A.C. (ed.) Clusters and Superclusters of Galaxies, p. 171.
Baum S.A., Heckman T., 1989, ApJ 336, 681
Begelman M. C., Cioffi D., 1989, ApJ 345, L21
Begelman M. C., Blandford R. D., Rees M. J., 1984, Rev. Mod. Phys. 56, 255
Bohringer H., Voges W., Fabian A.C., Edge A.C., Neumann D.M., 1993, MNRAS, 264, L25
Djorgovski S., Spinrad H., McCarthy P., Strauss M.A., 1985, ApJ 299, L1
Dressler A., Gunn J.E., 1983, ApJ 270, 7
Ecker R.D., Fanti R., Lari C., Parma P., 1978, Nature 276, 588
Ellis R.S., 1991, in: Bohringer H., Treumann R.A. (eds) Traces of the Primordial Structure in the Universe, Garching, MPE report 227, p.101
Fabian A.C.., 1994, ARA & A 32, 277
Feretti L., Gioia I.M., Giovannini G., Gregorini L., Padrielli L., 1984, A&A 139, 50
Ferland G. J., Netzer H., 1983, ApJ 264, 105
Giraud E., 1992, A&A 257, 501
Gopal-Krishna, Giraud E., Melnick J., Steppe H., 1992, A&A 254, 42
Gopal-Krishna, Giraud E. Melnick J., della Valle M., 1995, A&A, accepted
Guiderdoni B., Rocca-Volmerange B., 1988, A&AS 74, 185
Gull S.F.,Northover K.J.E., 1973, Nature 244, 80
Gunn J.E., 1979, in: Hazard C., Mitton S. (eds) Active Galactic Nuclei, Cambridge University Press, p. 213
Guzzo L., Danziger I.J., Christiani S., Shaver P.A., 1988, in: Audouze J. et al. (eds) Large Scale Structures of the Universe, Kluwer, Dordrecht, p. 573

Halpern J.P., Steiner J.E., 1983, ApJ 269, L37
Heckman T.M., Lehnert M.D., van Breugel W., Miley G.K., 1991, ApJ 370, 78
Heckman T.M., Baum S. A., van Breugel W.J.M., McCarthy P., 1989, ApJ 338, 48
Heckman T.M. et al., 1986, ApJ 311, 526
Hernquist L., 1993, ApJ 409, 548
Hill G.J., Lilly S.J., 1991, ApJ 367, 1
Hu E.H., Songaila A., Cowie L.L., Stockton A., 1991, ApJ 368, 28
Kotanyi C.G., Eckers R.D., 1979, A&A 73, L1
Lilly S.J., Prestage R.M., 1987, MNRAS 225, 531
McCarthy P.J., 1993, ARA&A 31, 639
McCarthy, P.J., van Breugel, W., 1989, in: Meurs E., Fosbury R.A.E. (eds) Extranuclear Activity in Galaxies, ESO, Garching, p.55
McCarthy P. J., 1988, PhD Thesis, University of California, Berkeley
Meisenheimer K., Hippelein H., 1992, A&A 264, 455
Melnick J., Altieri B, Gopal-Krishna, Giraud E., 1993, A & A 271, L8
Melnick J., Gopal-Krishna, Giraud E., 1995, in preparation
Miley G. K., 1992, in: Benvenuti P. & Schreier E. (eds) Science with Hubble Space Telescope, ESO Conference and Workshop Proceedings 44, p. 1
Mollenhoff C., Hummel E., Bender R, 1992, A&A 255, 35
Rawlings S., Saunders R., Eales S., Mackay C.D., 1989, MNRAS 240, 701
Rees M. J., 1989, MNRAS 239, 1p
Rottgering H., 1993, PhD thesis, Rijksuniversiteit, Leiden
Sparks W.B., 1992, ApJ 399, 66
Spinrad H., 1986, PASP 98, 269
Stockton A., McKenty J.W., 1987, ApJ 316, 584
Tyson J.A., AJ 96, 1
van Breugel W.J.M., Heckman T.M., Miley G.K., 1984, ApJ 276, 79
van Breugel W., Miley G., Heckman T., Butcher H, Bridle A., 1985, ApJ 290, 496
van Breugel W.J.M., Heckman T.M., Miley G.K., Filippenko A.V., 1986, ApJ 311, 58
Yates M.G., Miller L., Peacock J.A., 1989, MNRAS 240, 129

This article was processed by the author using Springer-Verlag LaTeX A&A style file version 3.